Coherent population trapping linewidths for open transitions: Cases of different transverse laser intensity distribution

M. Radonjić, D. Arsenović, Z. Grujić, and B. M. Jelenković*
Institute of Physics, Pregrevica 118, 11080 Belgrade, Serbia
(Received 16 August 2008; published 4 February 2009)

We calculated the coherent population trapping (CPT) for the open $D1$ line transition $F_g=2\rightarrow F_g=1$ in ^{87}Rb by solving the time-dependent optical Bloch equations, integrating the results for the total excited state populations over atomic trajectories, and averaging over velocities (components perpendicular and parallel to the laser beam) and over atom incident angles to the laser beam. We obtained a square root dependence of the CPT linewidths as a function of the laser intensity for both steplike and Gaussian transverse beam profiles. The results obtained with the Gaussian transverse laser beam profile are in good agreement with recent experimental results. Results for both steplike and Gaussian profiles of the laser beam show asymptotic $1/\sqrt{d}$ dependence (d is the laser beam diameter) of the CPT linewidths, for a large range of the laser intensity.

DOI: 10.1103/PhysRevA.79.023805 PACS number(s): 42.50.Gy, 42.50.Nn, 42.65.−k

I. INTRODUCTION

When an atom is prepared in a coherent superposition of two states, coupled by near-resonant light fields to the common upper state (Λ configuration), the atom population can be trapped in a superposition of lower states, called a dark state. Hence, this phenomenon is called coherent population trapping (CPT) [1,2]. The origin of coherence trapping is the destructive interference between transitions from the two lower states. Due to the CPT phenomenon, the medium becomes transparent. This phenomenon of a medium becoming transparent to the light field under the simultaneous action of a second light field is called electromagnetically induced transparency (EIT). Typically, EIT is associated with increased transparency of the probe field in the presence of a strong pump field (here the probe and pump fields are the two arms of the Λ configuration). In that case, the origin of EIT is the pumping of atoms into the dark state by both a strong pump and a weak probe field. CPT plays an important role in many fields of modern physics. It is used for laser cooling of atoms below the recoil limit [3,4], and for trapping of atoms in optical lattices [5].

Narrow CPT linewidths have important applications. CPT offers an alternative technique to bulky, complex, and heavy atomic clocks and frequency standards and to highly sensitive magnetometers, even when compared to superconducting quantum interference devices. Chip-scale atomic clocks [6] and magnetometers [7] have already been realized. A CPT medium has a very steep dispersion function which plays a key role in slowing group velocity of atoms [8] which makes CPT media interesting for quantum-information applications [9–12].

A key feature of the CPT for the above applications is the resonance slope, determined by the resonance amplitude and width. A great deal of work has been done on investigating the dependence of CPT line shapes on important experimental parameters for alkali-metal atoms contained in glass cells with and without buffer gas. For the CPT between ground state hyperfine levels of alkali-metal atoms in buffer gas cells, several theoretical studies [13,14] obtained a linear dependence of the linewidths on the pump laser intensity. On the other hand, calculations in [15] have found that this dependence is linear in the laser intensity only at higher laser intensity. The linewidth is linear in the laser Rabi frequency at lower laser intensity, i.e., when the pump field Rabi frequency Ω satisfies $\Omega^2 \ll 2\gamma\omega_D^2/\Gamma$, where γ is the coherence relaxation rate, ω_D is the Doppler width, and Γ is the total spontaneous emission rate. Theoretical models [13–15] assume a Λ atomic scheme, a steady state solution of the optical Bloch equations, and single values for the relaxation rates of the populations and coherences between the ground hyperfine levels. The relaxation rates for coherences are constants determined either by the diffusion rate (buffer gas cells) or by the reciprocal of the atom transit time through the laser beam.

Several experiments [13,14,16,17], in buffer gas cells, supported the theoretical prediction that the CPT linewidths vary linearly as a function of the laser intensity. Typically, experiments were done at laser intensities below 100 μW/cm^2. On the other hand, experiments in vacuum cells by Ye and Zibrov [18] on the $D2$ line in Rb agree qualitatively with the results of [15] and show a square root dependence on the laser intensity below ~3 mW/cm^2 and a linear dependence at higher laser intensities. Different behavior, with increased intensity causing narrowing of CPT resonance linewidths, was presented in [19,20]. In Ref. [19], the CPT resonance linewidths, measured for the $F_g=2\rightarrow F_e=1$ transition of the ^{87}Rb $D1$ line, decrease for laser intensities above a few mW/cm^2. In Ref. [20], the CPT for the closed $F_g=1\rightarrow F_e=0$ transition of the $D2$ line in ^{87}Rb shows a linewidth decrease when the laser intensity is larger than 40 mW/cm^2. Such dependence, with the maximum for the linewidths at laser intensities near the saturation limit, was obtained for electromagnetically induced absorption in a Doppler-broadened medium [21]. On the other hand, recent results, published in [22], gave nonlinear but monotonically increasing dependence of the Hanle CPT and EIT for the $F_g=2\rightarrow F_e=1$ transition in the $D1$ line of ^{87}Rb as a function of the laser intensity.

*branaj@phy.bg.ac.yu

The theoretical results that we mentioned above are for steplike dependence of the laser intensity on the laser diameter. The laser profile in experiments is usually Gaussian. The effects of the transverse intensity profiles on CPT line shapes and linewidths were studied in [23,24] also for a simple Λ configuration, using a steady state solution of the optical Bloch equations and by integrating the analytical expression for the linewidths over the radial laser beam profile.

In this work we theoretically investigate the linewidths of the CPT between Zeeman sublevels of the ground hyperfine level, by solving time-dependent density matrix equations for the open $F_g=2\rightarrow F_e=1$ transition in the $D1$ line. All the levels interacting with the laser light are taken into account, as well as population losses to another ground state hyperfine level. Atom fluorescence as a function of the external magnetic field (Hanle CPT) is obtained after integrating over atom trajectories in the laser beam and averaging over (a) atom velocity components perpendicular and parallel to the laser beam, and (b) incident angles of the atom with respect to the laser beam. We point out that we do not use any phenomenological terms in the optical Bloch equations, like relaxation of Zeeman coherences. Calculations were done for both steplike and Gaussian transverse laser beam profiles, for the laser intensity ranging from 0.01 to 40 mW/cm^2. Our results for the CPT linewidths are compared with the experimental results. We have also found dependence of the CPT linewidths on the laser beam diameter, i.e., on average atom-laser interaction time. Studies of dependence of the CPT linewidths on the interaction time for an open transition were previously performed only for Doppler-free systems [25,26]. We are not aware that such a detailed model as ours was previously applied to a Doppler-broadened open atomic system interacting with light fields with different transverse profiles.

II. THEORETICAL MODEL

EIT resonances were calculated for the $D1$ line transition $F_g=2\rightarrow F_e=1$ of ^{87}Rb gas in a vacuum cell in Hanle configuration. The transition is open because excited states can decay to another ground state level, $F_g=1$. The quantization z axis is chosen to be parallel to the external magnetic field. Zeeman sublevels of both the ground and the excited hyperfine states are coupled by a linearly polarized laser beam propagating along the z axis. The laser frequency ω_0 is chosen to be resonant with the specified transition. Equations for the density matrix elements connected with the $F_g=1$ ground level can be excluded since that level is not coupled by the laser. Although we consider a Doppler-broadened medium, inclusion of higher excited levels into the analysis is not necessary, as will be shown later. Under the assumption of purely radiative relaxation and in the rotating wave approximation, the optical Bloch equations (OBEs) for the density matrix of a moving atom have the form

$$\dot{\rho}_{e_ie_j}=i(\omega_{e_j}-\omega_{e_i})\rho_{e_ie_j}-\Gamma\rho_{e_ie_j}+\frac{i}{\hbar}\sum_{k=-F_g}^{F_g}(\tilde{\rho}_{e_ig_k}V_{+g_ke_j}-V_{-e_ig_k}\tilde{\rho}_{g_ke_j}), \tag{1a}$$

$$\dot{\tilde{\rho}}_{e_ig_j}=i(\omega_L-\omega_{e_i}+\omega_{g_j})\tilde{\rho}_{e_ig_j}-\frac{\Gamma}{2}\tilde{\rho}_{e_ig_j}+\frac{i}{\hbar}\sum_{k=-F_e}^{F_e}\rho_{e_ie_k}V_{-e_kg_j}-\frac{i}{\hbar}\sum_{k=-F_g}^{F_g}V_{-e_ig_k}\rho_{g_kg_j}, \tag{1b}$$

$$\begin{aligned}\dot{\rho}_{g_ig_j}&=i(\omega_{g_j}-\omega_{g_i})\rho_{g_ig_j}+\frac{i}{\hbar}\sum_{k=-F_g}^{F_g}(\tilde{\rho}_{g_ie_k}V_{-e_kg_j}-V_{+g_ie_k}\tilde{\rho}_{e_kg_j})\\&+(-1)^{i+j}(2F_e+1)\Gamma_{F_e\rightarrow F_g}\\&\times\sum_{q=-1}^{1}\rho_{e_{i+q}e_{j+q}}\begin{pmatrix}F_e & 1 & F_g\\ j+q & -q & -j\end{pmatrix}\begin{pmatrix}F_e & 1 & F_g\\ i+q & -q & -i\end{pmatrix},\end{aligned} \tag{1c}$$

where the subscripts e and g refer to the excited and the ground hyperfine levels, respectively. For our atomic system $F_e=1$ and $F_g=2$. Diagonal density matrix elements $\rho_{e_ie_i}$ ($\rho_{g_jg_j}$) are populations of e_i (g_j) Zeeman sublevels, while off-diagonal elements $\rho_{e_ie_j}$ ($\rho_{g_ig_j}$) are Zeeman coherences between e_ie_j (g_ig_j) sublevels. Fast oscillations of the optical coherences $\rho_{e_ig_j}$ between e_i and g_j sublevels were eliminated by standard substitution $\rho_{e_ig_j}=\tilde{\rho}_{e_ig_j}e^{-i\omega_Lt}$, where $\omega_L=\omega_0(1-v_\parallel/c)$ is the Doppler-shifted laser frequency and $v_\parallel$ is the magnitude of the atomic velocity component parallel to the laser direction. Energies of excited (ground) Zeeman sublevels e (g) with magnetic quantum numbers m_e (m_g) are given by $\hbar\omega_{e(g)}=\hbar\omega_{e_0(g_0)}+\mu_Bg_{F_{e(g)}}m_{e(g)}B$, where μ_B is the Bohr magneton and $g_{F_{e(g)}}$ is the Landé factor for the hyperfine levels. Γ represents the total spontaneous emission rate from each excited sublevel and for the ^{87}Rb $D1$ line it has the value $2\pi\times 5.746$ MHz. $\Gamma_{F_e\rightarrow F_g}$ is the decay rate from F_e to one F_g ground hyperfine level. It can be expressed in terms of Γ as

$$\Gamma_{F_e\rightarrow F_g}=(2J_e+1)(2F_g+1)\begin{Bmatrix}J_g & J_e & 1\\ F_e & F_g & I_g\end{Bmatrix}^2\Gamma, \tag{2}$$

and it obeys the sum rule $\Sigma_{F_g'}\Gamma_{F_e\rightarrow F_g'}=\Gamma$. The openness of the atomic system is quantitatively given by the ratio $\Gamma_{F_e\rightarrow F_g}/\Gamma$, which is less than 1 for open and exactly 1 for closed systems.

In a general case, the laser electrical field is given by

$$\mathbf{E}(\mathbf{r})=\mathbf{e}_xE_{0x}(\mathbf{r})\cos(\omega_Lt)+\mathbf{e}_yE_{0y}(\mathbf{r})\cos(\omega_Lt+\varphi^{yx}). \tag{3}$$

For symmetry reasons it is better to express the laser electrical field in terms of the spherical basis unit vectors $\mathbf{u}_{\pm 1}=(\mp\mathbf{e}_x-i\mathbf{e}_y)/\sqrt{2}$,

$$\mathbf{E}=\mathbf{u}_1(E_{1,+}e^{i\omega_Lt}+E_{1,-}e^{-i\omega_Lt})+\mathbf{u}_{-1}(E_{-1,+}e^{i\omega_Lt}+E_{-1,-}e^{-i\omega_Lt}), \tag{4}$$

where we used the notation $E_{\pm 1,\pm}=(\mp E_{0x}+ie^{\pm i\varphi^{yx}}E_{0y})/(2\sqrt{2})$. The terms $V_{\pm g_ie_j}$ in the OBEs are of the form

$$V_{\pm g_i e_j} = -\mu_{g_i e_j,-1} E_{-1,\pm} - \mu_{g_i e_j,1} E_{1,\pm}. \tag{5}$$

Here $\mu_{g_i e_j,q}$ is the electric dipole matrix element between the ground and excited states $|g_i\rangle \equiv |F_g m_{g_i}\rangle, |e_j\rangle \equiv |F_e m_{e_j}\rangle$, respectively, and it can be calculated as

$$\mu_{g_i e_j,q} = \langle F_g m_{g_i} | e\mathbf{u}_q \cdot \mathbf{r} | F_e m_{e_j}\rangle \tag{6}$$

$$= \langle J_g \| e\mathbf{r} \| J_e\rangle (-1)^{J_g+I_g+m_{g_i}} \times \sqrt{(2F_g+1)(2F_e+1)(2J_g+1)} \times \begin{Bmatrix} J_g & J_e & 1 \\ F_e & F_g & I_g \end{Bmatrix} \begin{pmatrix} F_e & 1 & F_g \\ m_{e_j} & q & -m_{g_i} \end{pmatrix}, \tag{7}$$

where $\langle J_g \| e\mathbf{r} \| J_e\rangle$ is the reduced matrix element of the electric dipole operator between arbitrary ground and excited states. In our case $J_g = J_e = 1/2$ and the corresponding value is taken from [27]. Due to the relation $\mu^*_{e_j g_i,q} = (-1)^q \mu_{g_i e_j,-q}$, the terms $V_{\pm e_j g_i}$ are completely determined by the terms $V_{\mp g_i e_j}$.

The density matrix calculated from the OBEs strongly depends on the spatial transverse profile of the electrical field. We performed calculations using steplike and Gaussian cylindrically symmetric profiles. In our theoretical treatment, the effects of the laser propagation and variation of its intensity along the Rb cell are neglected. It is shown in Ref. [28] that under real experimental conditions and for a range of laser intensities as in our calculations, the ratio of transmitted and input laser intensities is 60–75 %. Taking into account reflection in the front and back windows of the cell, we estimate that the average laser intensity in the cell is typically 80–90 % of the intensity that enters the Rb medium. The dependence of the laser intensity on the radial distance r from the beam center can be written as

$$I(r) = I_0 f(r/r_0), \tag{8}$$

where I_0 is the maximal intensity and $f(r/r_0)$ is a profile function which is chosen such that the profiles have the same total laser power P,

$$P = \int_0^\infty 2\pi r\, I_0 f(r/r_0) dr = I_0 \pi r_0^2. \tag{9}$$

r_0 is what we consider as the beam radius. For the steplike profile we take

$$f(r/r_0) = \begin{cases} 1, & r \leq r_0, \\ 0, & r > r_0, \end{cases} \tag{10}$$

while for the Gaussian profile we choose

$$f(r/r_0) = \exp(-r^2/r_0^2). \tag{11}$$

It can be argued without an explicit analysis that the resonance width for the Gaussian profile must be smaller than in the case of the steplike profile. For the Gaussian beam, the intensity reaches its maximal value I_0 only at the very center of the beam, while for the steplike profile intensity I_0 is present all over the beam. Thus, in the steplike profile all atoms see the same intensity, whereas for the Gaussian beam atoms in the outer regions are exposed to much lower laser intensity contributing to an overall line shape with narrower profiles.

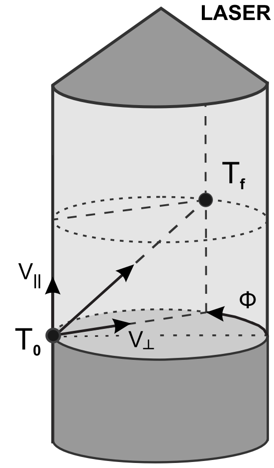

FIG. 1. Atom traversing laser beam.

The observed resonances in CPT and EIT experiments are probabilistic averages of contributions due to many individual, mutually noninteracting atoms. Rb atoms traverse the laser beam on different paths with different velocities. The atomic trajectory (line segment $\overline{\mathbf{T}_0\mathbf{T}_f}$ shown in Fig. 1) is completely determined by its velocity vector and starting position. The velocity component perpendicular to the laser beam, $\mathbf{v}_\perp$, is completely given by its magnitude $v_\perp$ and the angle ϕ as presented in Fig. 1.

The angle ϕ determines the atomic trajectory plane (which influences the spatial dependence of the electrical field experienced by a transiting atom) and also, together with $v_\perp$, the interaction time. From the point of view of the moving atom, the electrical field varies and the rate of variation depends on $v_\perp$. Suppose that the atomic trajectory has perpendicular projection given by $\mathbf{r}_\perp(t) = \mathbf{r}_{0\perp} + \mathbf{v}_\perp t$, where $\mathbf{r}_{0\perp}$ is the perpendicular component of the atom position vector at $t=0$. At time instant t, the electrical field seen by the atom is

$$\mathbf{E}(\mathbf{r}_\perp(t)) = \mathbf{E}(\mathbf{r}_{0\perp} + \mathbf{v}_\perp t). \tag{12}$$

The parallel velocity component $\mathbf{v}_\parallel$ affects the Doppler shift in the laser frequency seen by the atom. Besides the beam profiles, the parameters that determine the solutions of time-dependent Bloch equations are the maximal intensity I_0, the magnitudes of the atomic velocity components $v_\perp$ and $v_\parallel$, the angle ϕ, and the axial magnetic field B. It is worth noting that the temporal dependence for a given $v_\perp$ yields a spatial dependence in analogy with Eq. (12). For a suitably chosen set of those parameters, the OBEs were solved with initial conditions $\rho_{g_i g_j}(\mathbf{T}_0) = \frac{1}{8}\delta_{ij}$, $\rho_{e_i g_j}(\mathbf{T}_0) = 0$, $\rho_{e_i e_j}(\mathbf{T}_0) = 0$, obtaining the spatial dependence of the density matrix along corresponding trajectories. We use the fluorescence emitted from an atom as the measure of the effective absorption. Since all excited states decay at the same rate, the fluorescence is directly proportional to the total excited state population,

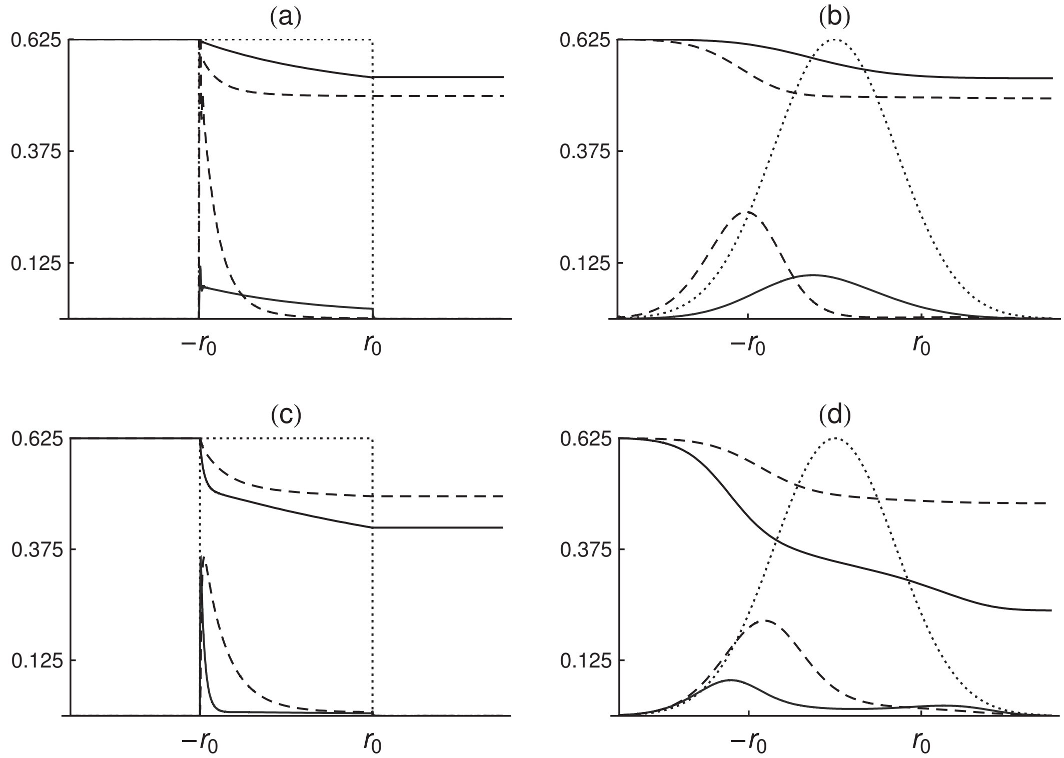

FIG. 2. Calculated spatial dependence of the total Zeeman sublevel populations of the ground $F_g=2$ (two upper curves in each figure) and the excited $F_e=1$ (two lower curves in each figure) hyperfine levels for a single atom. (a) and (b) show the effects of the laser intensity for $I_0=0.5$ mW/cm^2 (solid line) and $I_0=5$ mW/cm^2 (dashed line). Results are for $v_\perp=300$ m/s, $v_\parallel=5$ m/s. (c) and (d) show the effects of the perpendicular velocity component for $v_\perp=50$ m/s (solid line) and $v_\perp=300$ m/s (dashed line). Results are for $I_0=0.5$ mW/cm^2, $v_\parallel=0$ m/s. Beam profiles are shown in dotted lines and have $r_0=1.25$ mm. Excited level populations are multiplied by 25 in the case of a steplike and by 50 in the case of a Gaussian profile. $B=20$ mG. The atom enters the laser beam from the left.

$$f(B;\phi,v_\perp,v_\parallel,\mathbf{r}) = \Gamma \sum_{i=-F_e}^{F_e} \rho_{e_ie_i}(B;\phi,v_\perp,v_\parallel,\mathbf{r}), \quad \mathbf{r} \in \overline{\mathbf{T}_0\mathbf{T}_f}. \tag{13}$$

To obtain the final result, the CPT line profile, i.e., the fluorescence as a function of the external magnetic field, Eq. (13) has to be integrated along the atom trajectory, and then averaged over its velocity components and the angle ϕ. The following figures show the results of intermediate steps taken toward the CPT line profile. Through the results of such intermediate steps we justify the necessity to deal with time-dependent OBEs and take into account the real atomic system, real laser beam profile, and distribution of atomic velocities and incident angles with respect to the laser beam.

In Fig. 2 we show the spatial variation of the total population of the ground and the excited hyperfine states for the atom with specific values of the perpendicular $v_\perp$ and of the parallel $v_\parallel$ velocity components, for two laser intensities. These results were obtained for atoms traversing the laser beam along its diameter ($\phi=0$), and for an axial magnetic field $B=20$ mG. As the dotted lines indicate, the left sides are for the steplike while the right sides are for the Gaussian transverse laser beam profile.

It is evident that the atomic population of excited and ground states vary differently, both qualitatively and quantitatively, along the two laser beam profiles. After entering the laser beam, some fraction of the excited atoms decays into the uncoupled hyperfine level $F_g=1$, which results in population loss. The atoms decaying back to the $F_g=2$ hyperfine level can populate the dark state composed of Zeeman sublevels. The dark state is intensity dependent and ideally noncoupled only when there is no magnetic field. Therefore, when the intensity does not change rapidly and the magnetic field is sufficiently small, something like a steady state can be reached. In that case one part of the initial ground state population is pumped into an uncoupled second hyperfine level while the rest is in an almost noncoupled dark state. At $B=20$ mG, because atoms can be excited from the dark state, the population varies continuously while the atom is illuminated by the laser beam. Changes in the populations are much more rapid for steplike beam profiles. In a Gaussian beam, atoms are at first slowly pumped out from the $F_g=2$ level, resulting in the fluorescence peak being delayed until the atom reaches higher light intensities of the Gaussian beam. Also, optical pumping is lower and overall fluorescence is higher for faster atoms. It is apparent that level populations and CPT linewidths are influenced by the atomic motion all the time that the atom is in the laser beam. For $B\neq 0$ and high laser intensity, only populations for slow atoms can reach the steady state [Figs. 2(a) and 2(b)] due to the loss of population to the uncoupled ground state hyperfine level. Hence, in order to have a proper description and take into account the radial profile of the laser beam, it is

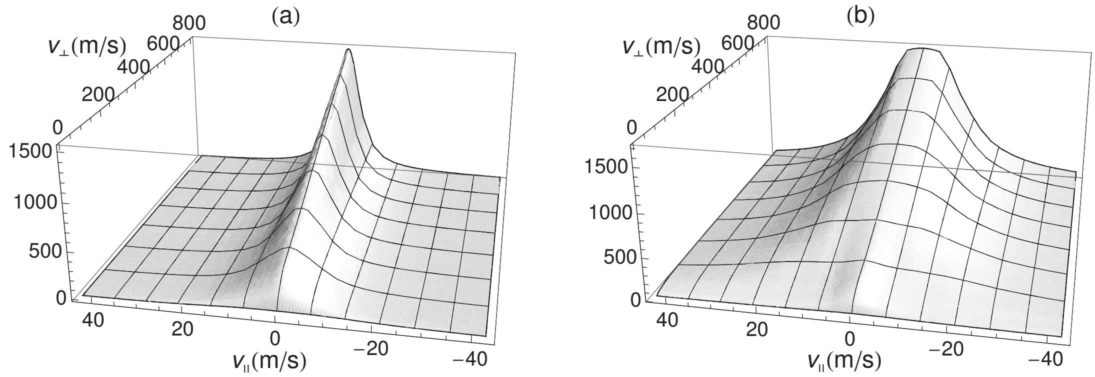

FIG. 3. Fluorescence integrated along trajectory (in arbitrary units) as a function of perpendicular $v_\perp$ and parallel $v_\parallel$ atom velocity components in the case of a Gaussian transverse beam profile. (a) is obtained for $I_0=0.5\ \mathrm{mW/cm^2}$ while (b) is for $I_0=5\ \mathrm{mW/cm^2}$. $B=20$ mG, $\phi=0$.

necessary to deal with time-dependent OBEs.

The total detected fluorescence comes from atoms interacting with the laser at the time of detection. Consequently, (13) must be integrated along the trajectory $\overline{\mathbf{T}_0\mathbf{T}_f}$,

$$\bar{f}(B;\phi,v_\perp,v_\parallel)=\int_{\mathbf{T}_0}^{\mathbf{T}_f} dr\, f(B;\phi,v_\perp,v_\parallel,\mathbf{r}). \tag{14}$$

Figure 3 shows the velocity dependence of the fluorescence integrated along the trajectory [Eq. (14)] in the case of a Gaussian profile for two laser intensities. A similar result is obtained for the steplike profile of the laser beam.

The trajectory-integrated fluorescence increases with $v_\perp$, i.e., with decrease of the time spent by the atom in the laser beam. Due to Doppler detuning, only atoms with the parallel velocity component inside a narrow range around $v_\parallel=0$ give a significant contribution to the fluorescence, as seen in Fig. 3. The contribution of atoms having large detuning is, in addition, greatly reduced due to the Maxwell-Boltzmann velocity distribution. When the values of B, ϕ, and $v_\perp$ are kept constant, the product of $\bar{f}(B;\phi,v_\perp,v_\parallel)$ and the weight corresponding to $v_\parallel$ in the Maxwell-Boltzmann distribution (i.e., a Doppler-detuning profile) is an even a bell-shaped function of $v_\parallel$. The contribution to the total fluorescence of atoms having larger $|v_\parallel|$ increases with the laser intensity, resulting in a wider Doppler detuning profile. This is evident from the results in Fig. 3 and we quantify this fact in Fig. 4. The solid (dashed) line shows the values of $|v_\parallel|$ for which the Doppler-detuning profile is reduced to 1/2 (1/1000) of the value corresponding to atoms with $v_\parallel=0$. In other words, the solid (dashed) curve in Fig. 4 is the half width at half (one-thousandth) maximum of the Doppler-detuning profile at a given laser intensity. Both curves are shown to indicate how rapidly the Doppler-detuning profile decreases with $v_\parallel$. Figure 4 supports our model assumption that we do not need to take into account other excited levels. Namely, even for the laser intensity $I_0=400\ \mathrm{mW/cm^2}$, the dashed curve comes up to the value of $|v_\parallel|\leqslant 540$ m/s. The corresponding frequency detuning is about 680 MHz which is still less than the 815 MHz splitting between the hyperfine level $F_e=1$ and the closest excited hyperfine level $F_e=2$. Almost the same result is obtained for a steplike beam profile. The value of 170 m/s for $v_\perp$, used for the calculations in Fig. 4, is chosen as the most probable value for the perpendicular velocity component.

After integrating over the trajectory, $\bar{f}(B;\phi,v_\perp,v_\parallel)$ was averaged over all velocity component magnitudes and angles,

$$\bar{F}(B;\phi)=\int_0^\infty dv_\perp W_\perp(v_\perp)\int_{-\infty}^{\infty} dv_\parallel W_\parallel(v_\parallel)\bar{f}(B;\phi,v_\perp,v_\parallel), \tag{15a}$$

$$F(B)=\int_0^{2\pi} d\phi\cos(\phi)W_\phi(\phi)\bar{F}(B;\phi). \tag{15b}$$

The additional term $\cos(\phi)$ in Eq. (15b) is due to the fact that the flux of atoms entering into the beam at angle ϕ is equal to the incident flux (isotropic by assumption) multiplied by $\cos(\phi)$. For the integration in (15a) and (15b) we assume a Maxwell-Boltzmann distribution of atomic velocities in the cell,

$$W(\mathbf{v})=W_\parallel(v_\parallel)W_\perp(v_\perp)W_\phi(\phi), \tag{16a}$$

with

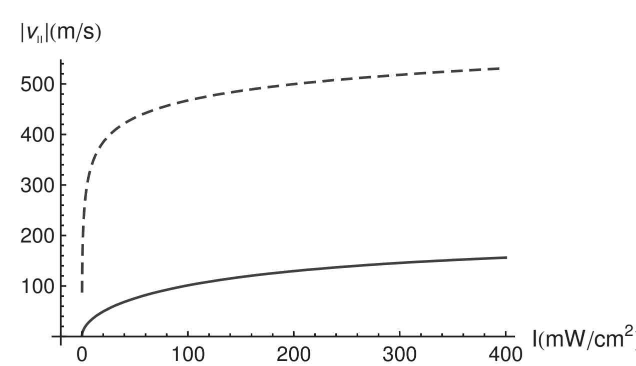

FIG. 4. Intensity dependence of parallel velocity components for which the Doppler-detuning profile reaches 1/2 (solid line) and 1/1000 (dashed line), respectively, of its peak value for $v_\parallel=0$. Beam profile is Gaussian. $B=20$ mG, $\phi=0$, $v_\perp=170$ m/s.

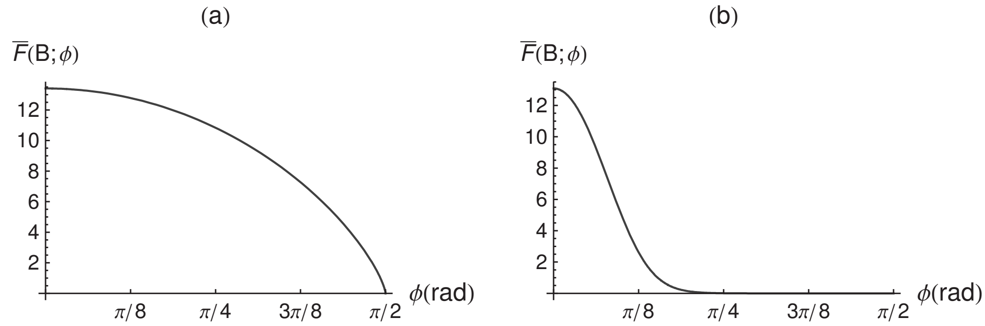

FIG. 5. Fluorescence given in arbitrary units, integrated along the atom trajectory and velocity components as a function of angle ϕ in the case of steplike (a) and Gaussian (b) transverse beam profile. Both plots are obtained for I_0=0.5 mW/cm^2 and B=20 mG.

$$W_{\|}(v_{\|}) = \frac{1}{u\sqrt{\pi}} e^{-(v_{\|}/u)^2}, \tag{16b}$$

$$W_{\perp}(v_{\perp}) = \frac{2v_{\perp}}{u^2} e^{-(v_{\perp}/u)^2}, \tag{16c}$$

$$W_{\phi}(\phi) = \frac{1}{2\pi}, \tag{16d}$$

where $u=(2k_BT/m)^{1/2}$ is the most probable velocity.

By performing velocity integrations of Eq. (15a) we get the contribution due to atoms moving at angle ϕ with respect to the laser beam diameter at $\mathbf{T}_0$ [Fig. 1] with all possible velocities. The dependence of $\bar{F}(B;\phi)$ on the angle ϕ for magnetic field B=20 mG is presented in Fig. 5. While the total fluorescence along ϕ=0 is similar for the two laser beam profiles, the overall $F(B)$ for the steplike profile is about two to three times greater than for the Gaussian profile. That is the case for all intensities and it verifies the necessity to consider trajectories at different angles ϕ. For fixed B it is found that the angular dependency of $\bar{F}(B;\phi)$ can be very well fitted to $A(B)[1-(2\phi/\pi)^2]^{p(B)}$ in the case of the steplike profile while for the Gaussian profile the fitting expression is more complex, $A_1(B)\exp[-p_1(B)\phi^2]+A_2(B)\exp[-p_2(B)\phi^3]$. At the present moment we do not have a theoretical explanation of these empirical results. The final integration is over angles ϕ (15b). The total fluorescence obtained in that manner is what we compare with experiment.

III. CPT RESONANCE LINEWIDTHS AND AMPLITUDES

The Hanle CPT resonances, calculated as a function of the external magnetic field, using Eq. (15b) are shown in Fig. 6. The left column is for a steplike and the right column is for a Gaussian laser beam profile. We present results for two laser intensities, 0.5 and 5 mW/cm^2, given by the lower and upper curves, respectively. The range of laser intensities in our calculations is between 0.01 and 40 mW/cm^2. The Hanle CPT curves were fitted using a superposition of a constant function and two Lorentzians in order to resolve the single-photon contribution (constant plus Lorentzian) from the pure CPT profile (the other Lorentzian). The dependence of the CPT linewidths, obtained as the full width at half maximum of the pure CPT profiles, as a function of the laser intensity is given in Fig. 7(a). In Fig. 7(b) we present laser intensity dependence of the CPT amplitudes. The amplitudes, dependent on the number of atoms put in a dark state, were normalized to the single-photon absorption amplitude. In Fig. 7(c) we show the slope of the resonances (the ratio between amplitude and linewidth) as a function of the laser intensity. The resonance slope is important for the performance of devices based on the CPT (see, for example, [17]). The solid curves are for the steplike beam profile, the dashed curves for the Gaussian profile.

As expected from analysis of the atomic level populations for selected parameters [Fig. 2], the two laser beam profiles give different results for amplitudes, linewidths, and slopes. The difference is particularly large for linewidths, since the Gaussian beam profile gives much narrower resonances. In both cases the linewidths are found to be proportional to the square root of intensity. The contrast of the resonances becomes higher than 0.5 at intensities of a few mW/cm^2. The

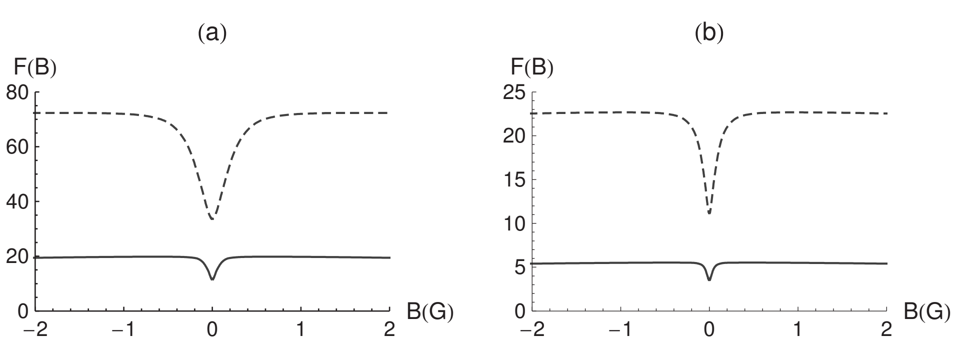

FIG. 6. Hanle CPT resonances for (a) steplike and (b) Gaussian transverse beam. Laser beam intensities are 0.5 mW/cm^2 (lower curves, solid lines) and 5 mW/cm^2 (upper curves, dashed lines).

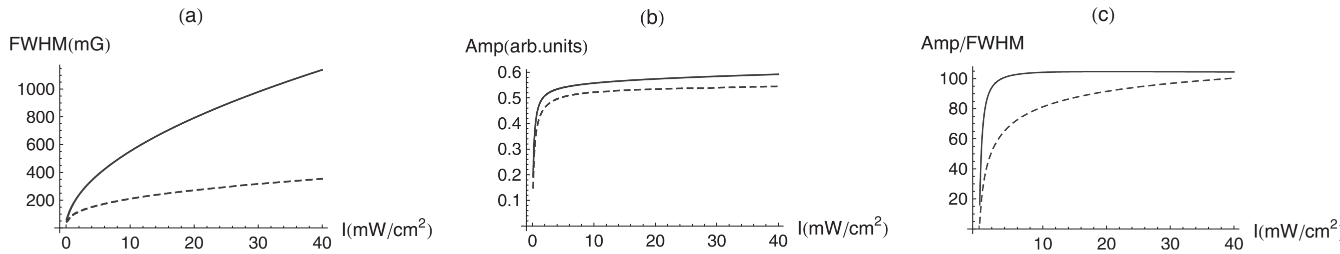

FIG. 7. CPT (a) linewidths, (b) amplitudes, and (c) amplitude/width ratio for step (solid lines) and Gaussian (dashed lines) laser beam radial profiles. CPT amplitudes are normalized to single-photon absorption amplitude.

amplitudes are in both cases a nonlinear but monotonic function of the laser intensity, being higher for the steplike profile.

Our results obtained with inclusion of a Gaussian laser beam profile might explain the previous discrepancy between calculations and experiment as found in Ref. [18]. In [18], Hanle CPT was calculated and measured for the $D2$ line $F_g=2 \rightarrow F_e=1$ transition in ^{87}Rb. The difference between the intensity dependence of the CPT linewidths for steplike and Gaussian laser beams, shown in Fig. 7(a) (this paper) is similar to the difference between theoretical and experimental linewidths shown in Ref. [18] in Fig. 7. In light of our calculations there is a possibility that the difference is a consequence of theoretical assumptions made in [18]—steady state solution of the OBEs and steplike beam profile. Figure 7(a) shows that the Gaussian profile, while generating narrower CPT linewidths, does not qualitatively change the dependence of the linewidths on the laser intensity with respect to the steplike profile. In Refs. [23,24], it is shown that the Gaussian profile generates narrower CPT resonances between hyperfine levels and gives a different dependence of the linewidths on the laser intensity than the steplike profile. In [23], for higher intensities, the Gaussian profile gives a linear dependence as a function of the laser Rabi frequency, while the steplike profile gives a linear dependence as a function of the laser intensity. In [24], the two profiles give different dependences at lower laser intensity while at higher intensities (the sum of both laser intensities is much larger than the coherence relaxation rate normalized to the decay rate of the excited state) both profiles give near-linear dependence. It is important to note that both Refs. [23,24] consider alkali-metal atoms in buffer gas cells, which is a different system than the one we study.

In Figs. 8(a) and 8(b) we compare the results of our calculations to results in [22]. For the comparison with results in [22], we used a Gaussian laser beam profile with the radius of 1.25 mm in calculations, and extended the range of the laser intensity up to 400 mW/cm^2. Very good agreement between theory and experiment for the CPT linewidths is evident from the comparison in Fig. 8(a). There is no normalization of the two sets of data in Fig. 8(a). Our results do not show narrowing of the CPT at higher laser intensities as shown in [19]. The measured CPT amplitudes (given in arbitrary units in [22]) were normalized to match the calculated amplitude for the maximal laser intensity. Differences between measured and calculated amplitudes, presumably because our model does not include laser propagation and absorption in the cell, become larger at lower laser intensities where absorption of resonant laser light is higher.

Narrowing of the CPT resonances with increasing laser beam diameter, i.e., with the increase of the interaction time, is well known. Different methods are used to increase the interaction time, by adding a buffer gas, or by using coated cells. We obtained the CPT linewidth dependence on beam diameter given in Fig. 9, which is similar to previously predicted $1/\sqrt{t}$ asymptotical dependence of the linewidths [25,26], where t is the interaction time between the atom and the laser light. Those results were obtained using the time-dependent OBE for the open system without taking into account the Doppler broadening. As discussed in [25], the $1/\sqrt{t}$ narrowing law in open systems is a consequence of the quadratic dependence in the Raman detuning of the effective width of the noncoupled state due to the light irradiation and to the applied magnetic field. Our results support the extension of that conclusion and the $1/\sqrt{t}$ narrowing law to Doppler-broadened open systems.

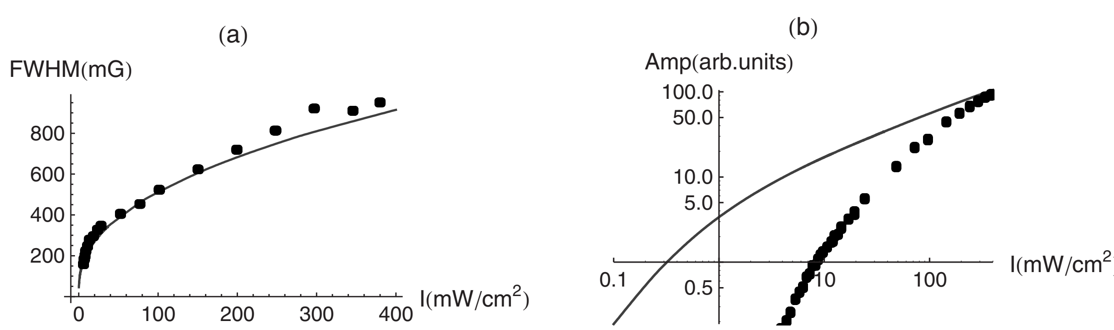

FIG. 8. Comparison of our calculation for Gaussian laser beam radial profile with experimental data from [22]. CPT (a) linewidths and (b) amplitudes. Solid lines represent our calculation while symbols correspond to measurements from Ref. [22]. Measured amplitudes are normalized to match the value calculated at highest intensity.

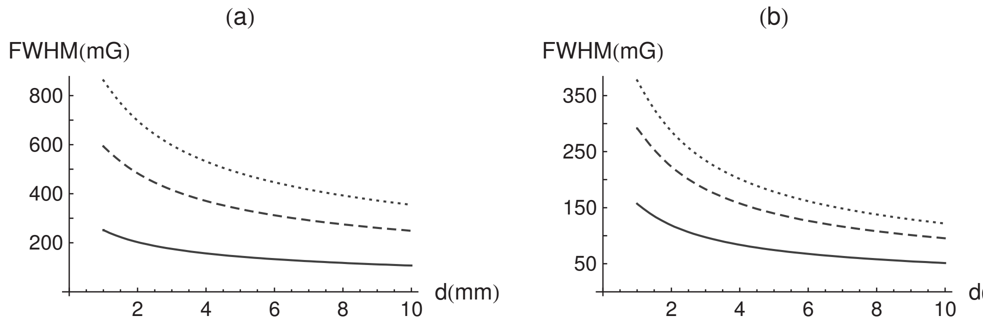

FIG. 9. Calculated dependence of linewidths on laser beam diameter for steplike (a) and Gaussian (b) beam profile. Solid, dashed, and dotted lines correspond to laser intensities $I_0=1$, 5, and 10 mW/cm^2, respectively.

IV. SUMMARY

A theoretical model that takes into account all atomic levels coupled by the laser light and optical pumping to the hyperfine level not coupled by the laser was used to calculate CPT between Zeeman sublevels of the $F_g=2$ hyperfine state of ^{87}Rb. The populations of ground and excited states change as long as the atom traverses the laser beam, for small axial magnetic field and up to moderately high laser intensity. This by itself presents a good argument that time-dependent solutions of the optical Bloch equations are preferable for the CPT in an open transition. Our detailed model gave a nonlinear, monotonically increasing CPT linewidth dependence proportional to the square root of laser intensity. The results can be compared with experiments with vacuum gas cells. The linewidths are considerably narrower for the Gaussian than for the steplike transverse profile of the laser beam. Different results for the linewidths for two laser beam profiles can explain the discrepancies between previous theory and experiment. Our results did not support experimental observations of laser intensity narrowing of the CPT resonance. We have shown very good agreement between our results and recent experiments for the intensity dependence of the Hanle CPT linewidths. Both steplike and Gaussian laser beam profiles gave $1/\sqrt{d}$ asymptotic dependence of the CPT linewidths on laser beam diameter d. This dependence remains for a wide range of the laser intensities. Our results suggest that the $1/\sqrt{t}$ asymptotic dependence (where t is the interaction time) of the CPT linewidths for open transitions in atomic beams also holds in Doppler-broadened media.

ACKNOWLEDGMENTS

We are thankful to Professor W. Gawlik for providing experimental data presented so far only in the thesis of S. Pustelny. This work was supported by the Ministry of Science of the Republic of Serbia, under Grant No. 141003.

[1] E. Arimondo, Prog. Opt. **35**, 257 (1996).
[2] S. E. Harris, J. E. Field, and A. Imamoglu, Phys. Rev. Lett. **64**, 1107 (1990).
[3] A. Aspect, E. Arimondo, R. Kaiser, N. Vansteenkiste, and C. Cohen-Tannoudji, Phys. Rev. Lett. **61**, 826 (1988).
[4] H. J. Metcalf and P. van der Straten, *Laser Cooling and Trapping* (Springer-Verlag, New York, 2001).
[5] A. Hemmerich, M. Weidemüller, T. Esslinger, C. Zimmermann, and T. Hänsch, Phys. Rev. Lett. **75**, 37 (1995).
[6] S. Knappe, V. Shah, P. D. D. Schwindt, L. Hollberg, J. Kitching, L. A. Liew, and J. Moreland, Appl. Phys. Lett. **85**, 1460 (2004).
[7] P. D. D. Schwindt, S. Knappe, V. Shah, L. Hollberg, J. Kitching, L. A. Liew, and J. Moreland, Appl. Phys. Lett. **85**, 6409 (2004).
[8] O. Schmidt, R. Wynands, Z. Hussein, and D. Meschede, Phys. Rev. A **53**, R27 (1996).
[9] C. H. van der Wal, M. D. Eisaman, A. André, R. L. Walsworth, D. F. Phillips, A. S. Zibrov, and M. D. Lukin, Science **301**, 196 (2003).
[10] A. M. C. Dawes, L. Illing, S. M. Clark, and D. J. Gauthier, Science **308**, 672 (2005).
[11] Irina Novikova, Alexey V. Gorshkov, David F. Phillips, Anders S. Sørensen, Mikhail D. Lukin, and Ronald L. Walsworth, Phys. Rev. Lett. **98**, 243602 (2007).
[12] M. D. Lukin, Rev. Mod. Phys. **75**, 457 (2003).
[13] J. Vanier, A. Godone, and F. Levi, Phys. Rev. A **58**, 2345 (1998).
[14] M. Erhard and H. Helm, Phys. Rev. A **63**, 043813 (2001).
[15] A. Javan, O. Kocharovskaya, H. Lee, and M. O. Scully, Phys. Rev. A **66**, 013805 (2002).
[16] M. Stahler, R. Wynands, S. Knappe, J. Kitching, L. Hollberg, A. Taichenachev, and V. Yudin, Opt. Lett. **27**, 1472 (2002).
[17] S. Knappe, R. Wynands, J. Kitching, H. G. Robinson, and L. Hollberg, J. Opt. Soc. Am. B **18**, 1545 (2001).
[18] C. Y. Ye and A. S. Zibrov, Phys. Rev. A **65**, 023806 (2002).
[19] S. Gateva, E. Alipieva, and E. Taskova, Phys. Rev. A **72**, 025805 (2005).
[20] W. Yi, Z. Ming-Sheng, and W. Yu-Zhu, Chin. Phys. **16**, 994 (2007).
[21] J. Dimitrijević, D. Arsenović, and B. M. Jelenković, Phys. Rev. A **76**, 013836 (2007).
[22] S. Pustelny, MS thesis, University of Krakow, 2003.
[23] F. Levi, A. Godone, J. Vanier, S. Micalizio, and G. Modugno,

Eur. Phys. J. D **12**, 53 (2000).
[24] A. V. Taichenachev, A. M. Tumaikin, V. I. Yudin, M. Stähler, R. Wynands, J. Kitching, and L. Hollberg, Phys. Rev. A **69**, 024501 (2004).
[25] F. Renzoni, A. Lindner, and E. Arimondo, Phys. Rev. A **60**, 450 (1999).
[26] F. Renzoni and E. Arimondo, Phys. Rev. A **58**, 4717 (1998).
[27] M. L. Harris, C. S. Adams, S. L. Cornish, I. C. McLeod, E. Tarleton, and I. G. Hughes, Phys. Rev. A **73**, 062509 (2006).
[28] M. M. Mijailovic, J. Dimitrijevic, A. J. Krmpot, Z. D. Grujic, B. M. Panic, D. Arsenovic, D. V. Pantelic, and B. M. Jelenkovic, Opt. Express **15**, 1328 (2007).